Langmuir

ARTICLE

pubs.acs.org/Langmuir

# Intraparticle Charge Delocalization of Carbene-Functionalized Ruthenium Nanoparticles Manipulated by Selective Ion Binding

Xiongwu Kang, Wei Chen,† Nathaniel B. Zuckerman, Joseph P. Konopelski, and Shaowei Chen*

Department of Chemistry and Biochemistry, University of California, 1156 High Street, Santa Cruz, California 95064, United States

Supporting Information

**ABSTRACT:** Olefin metathesis reactions of carbene-stabilized ruthenium nanoparticles were exploited for the incorporation of multiple functional moieties onto the nanoparticle surface. When the nanoparticles were cofunctionalized with 4-vinylbenzo-18-crown-6 and 1-vinylpyrene, the resulting particles exhibited fluorescence characteristics that were consistent with dimeric pyrene with a conjugated chemical bridge, with three peaks observed in the emission spectra at 391, 410, and 485 nm. The behaviors were ascribed to intraparticle charge delocalization between the pyrene moieties afforded by the conjugated Ru═carbene interfacial linkages. Notably, upon the binding of metal ions in the crown ether cavity, the emission intensity of the nanoparticle fluorescence was found to diminish at 485 nm and concurrently increase at 391 and 410 nm rather markedly, with the most significant effects observed with $K^+$. This was accounted for by the selective binding of 18-crown-6 to potassium ions, where the positively charged ions led to the polarization of the nanoparticle core electrons that was facilitated by the conjugated linkage to the metal surface and hence impeded intraparticle charge delocalization. Control experiments with a pyrene−crown ether conjugate (**2**) and with ruthenium nanoparticles cofunctionalized with 4-vinylbenzo-18-crown-6 and 1-allylpyrene suggested that the through-bond pathway played a predominant role in the manipulation of intraparticle electronic communication whereas the contributions from simple electrostatic interactions (i.e., through-space pathway) were minimal.

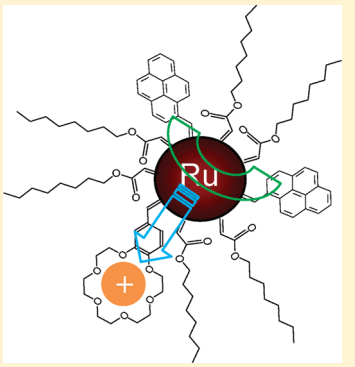


## INTRODUCTION

In recent years, surface-engineered metallic nanoparticles have attracted a great deal of attention because of their diverse potential applications in catalysis, nanoelectronics, photoluminescent devices, data storage, and so forth. Among these, monolayer-protected nanoparticles, in comparison with conventional materials, show unique advantages in that their optoelectronic properties can be readily manipulated not only by the chemical nature of the metallic cores and the surface functional ligands[1−3] but also by the metal−ligand interfacial bonding interactions. The latter has recently been manifested in a series of studies where we demonstrated that for ruthenium nanoparticles stabilized by metal−carbene $\pi$ bonds[4] or alkynyl fragments,[5] apparent intraparticle charge delocalization might occur as a consequence of the conjugated metal−ligand interfacial linkages. This unique phenomenon was exemplified by the apparent intervalence transfer between particle-bound, mixed-valence ferrocenyl moieties that was attested to by electrochemical and spectroscopic measurements. Such chemistry has also been exploited to manipulate the nanoparticle optical properties by incorporating fluorophores (e.g., pyrene, anthracene, etc.) onto the nanoparticle surface, where the photoluminescence characteristics were found to be analogous to those of the corresponding dimers with a conjugated chemical bridge.[6−8]

In these studies, intraparticle charge delocalization arose from the effective overlap between the $d_\pi$ orbital or the $p_\pi d_\pi$ hybrid of the Ru metal and the $\pi^*$ orbital of the ligand carbons[9,10] as well as from the conducting particle cores that served as the chemical linkage in bridging the functional moieties, as manifested in constrained density functional theory (CDFT) studies.[4,11,12] Within this context, the extent of intraparticle charge delocalization was found to be manipulated by the charge state of the nanoparticle cores by simple chemical reduction and oxidation, as demonstrated in optical and spectroscopic measurements.[13]

Herein, we extend the study of the manipulation of intraparticle charge delocalization by selective ion binding with crown ether moieties incorporated onto the nanoparticle surface by the Ru═carbene $\pi$ bond. This is to take advantage of the unique characteristics of crown ethers that form stable complexes with selective ions. It is envisaged that upon the binding of metal ions to the crown ether cavity, the resulting electrostatic charge will induce polarization of the electrons within the nanoparticle core that is facilitated by the conjugated linkage to the metal surface, leading to further deliberate manipulation of intraparticle extended conjugation between particle-bound functional moieties (Scheme 1). We will use carbene-stabilized ruthenium nanoparticles functionalized with pyrene moieties as examples and will examine the fluorescence characteristics of the nanoparticles in the presence of various metal ions. Specifically, as shown in Scheme 1, multiple copies of 4-vinylbenzo-18-crown-6 were incorporated onto the nanoparticle surface by olefin metathesis reactions,

**Received:** June 27, 2011
**Revised:** August 26, 2011
**Published:** September 06, 2011

and among the series of metal cations under study ($Li^+$, $Na^+$, $K^+$, and $Mg^{2+}$), $K^+$ exhibited the most drastic impact on the fluorescence characteristics of the pyrene-functionalized nanoparticles, consistent with the selectivity of the crown ether moiety toward $K^+$.

## EXPERIMENTAL SECTION

**Materials.** Ruthenium chloride ($RuCl_3$, 99+%, Acros), 1,2-propanediol (Acros), sodium acetate trihydrate ($NaAc \cdot 3H_2O$, MC&B), 4-vinylbenzo-18-crown-6 ($C_{18}H_{26}O_6$, 97%, Acros), lithium perchlorate ($LiClO_4$, 99.5%, Fisher Chemical), sodium perchlorate ($NaClO_4$, Fisher Chemical), potassium perchlorate ($KClO_4$, Fisher Chemical), magnesium perchlorate ($Mg(ClO_4)_2$, Aldrich Chemical), and extra-dry *N*,*N*-dimethylformamide (DMF, 99.8%, Aldrich) were used as received. All solvents were obtained from typical commercial sources and used without further treatment. Water was supplied by a Barnstead Nanopure water system (18.3 MΩ·cm).

The pyrene−crown ether conjugate (**2**) was prepared by Wittig reactions between triphenyl(pyren-1-ylmethyl)phosphonium bromide and 4′-formylbenzo[14] (**1**), as depicted in Scheme 2 and detailed in the Supporting Information.

**Functionalization of Ruthenium Nanoparticles.** The preparation of ruthenium nanoparticles has been detailed previously.[4,6,7,15] Experimentally, ruthenium nanoparticles protected by carbene fragments, which had a core diameter of 2.12 ± 0.72 nm as determined by transmission electron microscopy (TEM) measurements, were first synthesized by mixing freshly prepared ruthenium particles with octyl diazoacetate (ODA).[15] The resulting nanoparticles, which are referred to as Ru═C8, were then functionalized by olefin metathesis reactions with 4-vinylbenzo-18-crown-6 or a mixture of 4-vinylbenzo-18-crown-6 and 1-vinylpyrene or 1-allylpyrene (Scheme 3). The resulting functionalized particles were denoted as Ru═CE, Ru═VPyCE, and Ru═APyCE, respectively. The concentrations of the pyrene and crown ether moieties on the Ru nanoparticle surface were determined by $^1$H NMR spectroscopic measurements whereby the organic components were extracted after the Ru cores were dissolved by dilute KCN.[4,6] The spectra were included in the Supporting Information (Figure S1), where the integrated peak areas of the methyl protons of the original ODA ligands (0.9 ppm), the aromatic protons of the pyrene moieties (8.3 to 7.7 ppm), and the phenyl (7.0 to 6.8 ppm) and methylene protons (4.2 to 3.6 ppm) of the benzo-18-crown-6 ligands were used to calculate their concentrations on the nanoparticle surface. The results are summarized in Table 1.

**Spectroscopy.** $^1$H NMR spectroscopic data were acquired with a Varian Unity 500 MHz spectrometer. Fluorescence measurements were carried out with a PTI fluorospectrometer. In a typical procedure, 2 mL of a Ru═VPyCE nanoparticle solution at a concentration of 0.05 mg/mL in DMF was added to a quartz cuvette. A calculated amount of a metal salt analyte (1 M) in DMF was then injected into the cuvette with a Hamilton microliter syringe. Fluorescence spectra were collected after thorough mixing of the analyte with the nanoparticle solution. The same procedure was used in the measurements of Ru═APyCE nanoparticles and the monomeric pyrene−crown ether conjugate (**2**).

**Scheme 1. Carbene-stabilized Ruthenium Nanoparticles Functionalized with Vinylpyrene and 4-Vinylbenzo-18-crown-6 Moieties**[a]

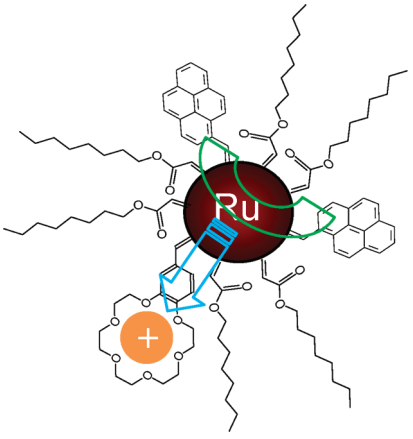


[a] The selective binding of cations to the crown cavity may impact the charge delocalization between pyrene moieties, as manifested in fluorescence measurements.

## RESULTS AND DISCUSSION

Previously, we demonstrated that when carbene-stabilized ruthenium (Ru═C8) nanoparticles were functionalized by olefin metathesis reactions with 1-vinylpyrene, the resulting nanoparticles exhibited fluorescence characteristics that were consistent with those of pyrene dimers with a conjugated chemical linker (−CH═CH−), suggesting effective intraparticle charge delocalization as a consequence of the conjugated interfacial linkages, whereas with 1-allylpyrene, the fluorescence profiles of the nanoparticles were akin to those of monomeric pyrene, indicative of the switch off of extended conjugation between the particle-bound pyrene moieties by the $sp^3$ carbon spacers.[6,7] Such a behavior was also observed for the Ru═VPyCE nanoparticles in the present study (Scheme 3). Figure 1 shows the excitation and emission spectra of Ru═VPyCE nanoparticles in DMF (black curves). It can be seen that the excitation spectra exhibited two major peaks at 284 and 350 nm and that the emission spectra featured three main peaks at 391, 410, and 485 nm, consistent with those observed previously with Ru═VPy nanoparticles.[6,7] This suggests that even in the presence of the (benzo)crown ether moieties, effective electronic interactions occurred between the pyrene moieties on the nanoparticle surface. More interestingly,

**Scheme 2. Synthesis of the Pyrene−Crown Ether Conjugate (2)**

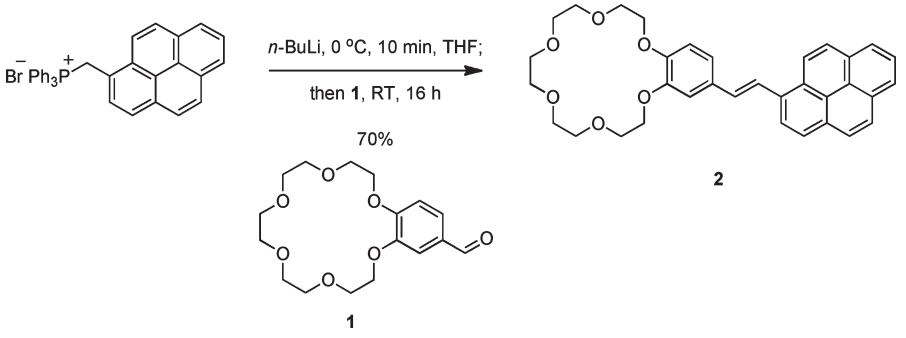

**Scheme 3. Olefin Metathesis Reactions of Carbene-Stabilized Ruthenium (Ru═C8) Nanoparticles with Vinyl-Terminated Functional Ligands**

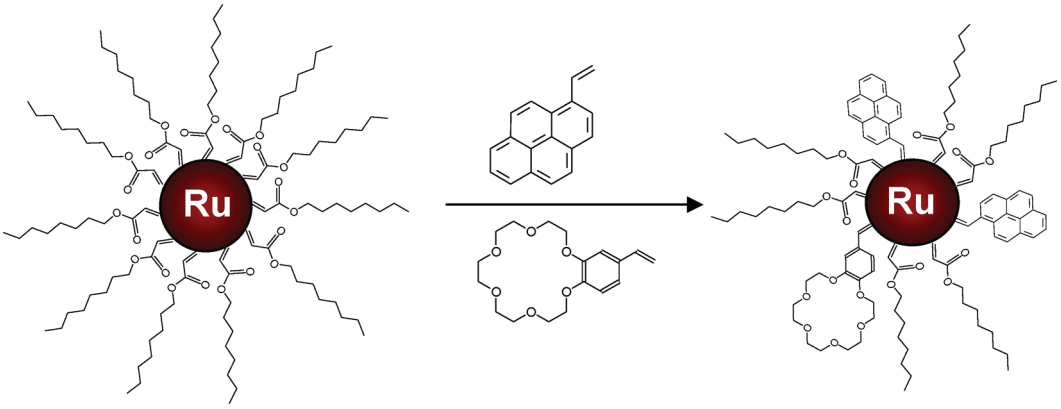


**Table 1. Concentrations of Crown Ether (CE) and Pyrene (Py) Moieties on the Ruthenium Nanoparticle Surface as Determined by $^1$H NMR Measurements**

| | Ru═CE (%) | Ru═VPyCE (%) | Ru═APyCE (%) |
|---|---|---|---|
| ODA | 69.6 | 48.0 | 32.0 |
| Py | | 40.5 | 40.0 |
| CE | 31.4 | 11.5 | 28.0 |

the fluorescence profiles of the Ru═VPyCE nanoparticles exhibited a rather sensitive variation with the addition of various metal ions: (A) $LiClO_4$, (B) $NaClO_4$, (C) $KClO_4$, and (D) $Mg(ClO_4)_2$. For instance, with the addition of $KClO_4$ (panel C), the emission intensity at 485 nm diminished markedly; concurrently, the emission at shorter wavelengths increased, with an isosbestic point at ca. 444 nm. Similar but less dramatic effects were observed with the addition of $Na^+$ (panel B), whereas for $Li^+$ (panel A) and $Mg^{2+}$ (panel D), the effects were even more subtle. Figure 2 depicts the variation of the emission peak intensity at (A) 391 and (B) 485 nm with the addition of various metal salts. It can be seen that at 10 mM the fluorescence intensity at 391 nm (panel A) increased by about 20% for $K^+$ and 11% for $Na^+$ and remained virtually unchanged for $Mg^{2+}$ (−2%) and $Li^+$ (−5%). At the same time, the intensity at 485 nm (panel B) decreased by about 10% for both $K^+$ and $Na^+$, 4% for $Li^+$, and 1% for $Mg^{2+}$. Overall, these observations suggest that the impacts of the metal ions on Ru═VPyCE fluorescenece decrease in the order of $K^+ > Na^+ > Li^+ \approx Mg^{2+}$.

It should be noted that the emission peak at 485 nm was characteristic of dimeric pyrene moieties that formed as a result of intraparticle extended conjugation, whereas the emission at 391 and 410 nm had mostly monomeric characters.[6,7] Therefore, the variation of the fluorescence profiles observed above with the Ru═VPyCE nanoparticles suggests that intraparticle charge delocalization between the pyrene moieties diminished with the addition of metal ions, most likely because of the specific binding of the metal ions to the crown ether cavities that led to the polarization of the nanoparticle core electrons. This is analogous to what we observed previously with alkynyl-passivated ruthenium nanoparticles where the discharging (oxidation) of the nanoparticle cores led to reduced electronic communication between the acetylene moieties and hence an enhancement of their bonding order.[13] In the present study, the binding of metal cations to the crown ether cavity on the nanoparticle surface lowered the energy of the nanoparticle core electrons through the conjugated vinylbenzo linkage (i.e., through-bond pathway) and thus diminished their participation in intraparticle charge delocalization such that the particle-bound pyrene moieties behaved increasingly independently, as observed experimentally. Furthermore, the fact that $K^+$ exhibited the most significant impact on the nanoparticle fluorescence characteristics may be accounted for by the selective binding of the crown ether that is dictated by the size of the cavity and the ion radius. For 18-crown-6, the crown ether cavity is optimal for potassium ions.[16−18]

In essence, with the incorporation of crown ether moieties into the nanoparticle protecting layer, the specific binding of metal ions may be exploited as an effective chemical gate in the regulation of the intraparticle charge delocalization between particle-bound pyrene groups.

It should be noted that the contribution is minimal from simple electrostatic interactions (i.e., through-space pathway) to the regulation of the electronic communication between the pyrene moieties on the Ru═VPyCE nanoparticle surface, as attested to by the control experiment with Ru═APyCE nanoparticles. Figure 3 shows the fluorescence spectra of Ru═APyCE with the addition of $K^+$ to the solution. It can be seen that the nanoparticle fluorescence profiles remained virtually invariant, although the concentration of the crown ether moieties on the nanoparticle surface (40.0%) was almost the same as that (40.5%) on Ru═VPyCE (Table 1). Previously, we showed that for Ru═APyCE nanoparticles the insertion of $sp^3$ carbon spacers into the chemical bridge effectively shut off the intraparticle electronic communication and hence the nanoparticles exhibited fluorescence profiles that were consistent with those of monomeric pyrene.[6,7] The fact that the fluorescence spectra remained unchanged with the addition of up to 10 mM $K^+$ strongly suggests that electrostatic interactions alone did not lead to an apparent enhancement of the nanoparticle fluorescence. That is, the through-space pathway is much less effective.

Furthermore, one may notice that with the cofunctionalization of the nanoparticles by both pyrene and (benzo)crown ether functional moieties (Scheme 3) intraparticle extended conjugation may emerge not only between the pyrene groups as observed above in Figure 1 but also between the (benzo)crown ether groups and between the pyrene and (benzo)crown ether

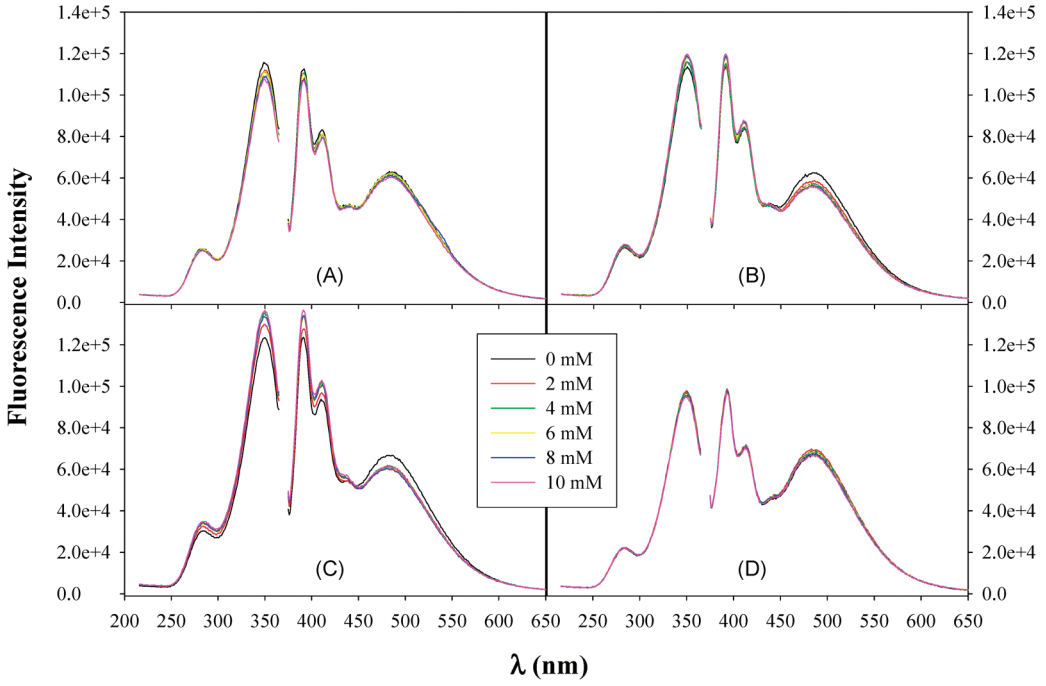


**Figure 1.** Excitation and emission spectra of Ru═VPyCE nanoparticles (2 mL, 0.05 mg/mL in DMF) with the addition of various amounts of metal salts in DMF (0.1 M): (A) $LiClO_4$, (B) $NaClO_4$, (C) $KClO_4$, and (D) $Mg(ClO_4)_2$. The final concentrations of the metal ion are listed in the legend. The excitation wavelength is set at 349 nm.

moieties. In fact, for ruthenium nanoparticles functionalized with (benzo)crown ether alone (i.e., Ru═CE nanoparticles, Table 1), apparent fluorescence can be observed as well, as depicted in Figure 4. It can be seen that the excitation spectra exhibit a peak at 345 nm and the emission spectra show a peak at 392 nm, which is attributed to the conjugation between the vinylbenzo moieties bound to the nanoparticle surface (Scheme 3) leading to the formation of a stilbene-like structure ($-C_6H_4-CH=CH-C_6H_4-$). In fact, the fluorescence characteristics are analogous to those observed for stilbene derivatives.[19,20]

Notably, upon the addition of various metal ions ($LiClO_4$, $NaClO_4$, $KClO_4$, and $Mg(ClO_4)_2$), the fluorescence intensity exhibited an apparent increase, as depicted in Figure 5. For instance, at 8 mM, the nanoparticle fluorescence intensity increased by 36 ($K^+$), 32 ($Na^+$), 34 ($Li^+$), and 27% ($Mg^{2+}$). Again, this may be attributable to the selective binding of metal ions by the crown ether moieties. In the absence of metal ions, the fluorescence was partially quenched by the transfer of the HOMO electrons of the crown ether moieties to the stilbene analogs. Upon the binding of the metal ions to the cavity, the energy of the crown ether HOMO electrons was lowered, which impeded the photoinduced electron transfer leading to the recovery of the particle fluorescence.[21] In fact, among the series of metal ions, $K^+$ stood out with the largest increase of particle fluorescence, consistent with the selective binding of $K^+$ by the 18-crown-6 cavities. Thus, one may argue that the enhancement of Ru═VPyCE fluorescence by the addition of metal ions, as observed in Figure 1, may also include the contributions of the extended conjugation between the (benzo)crown ether moieties because the fluorescence profiles overlap extensively. However, from Figure 4 it can be seen that the fluorescence emission of the Ru═CE nanoparticles is at least

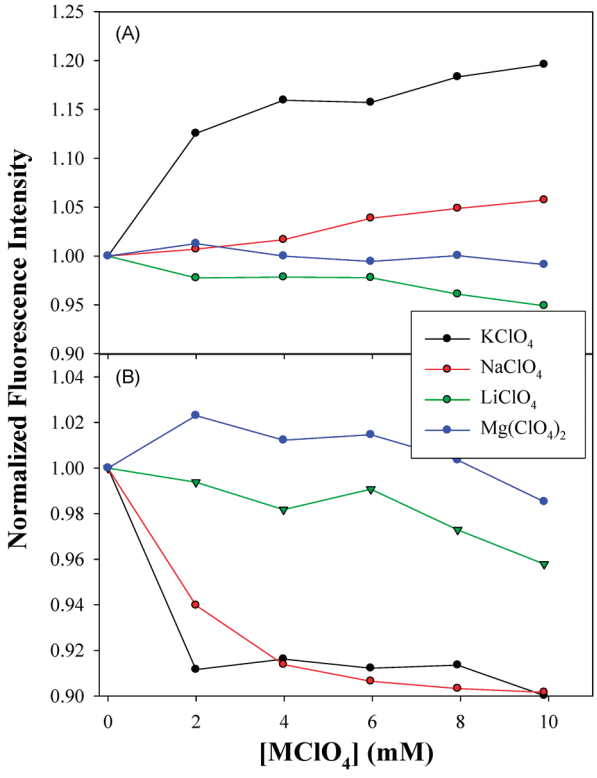


**Figure 2.** Variation of the emission intensity of the Ru═VPyCE nanoparticles with the addition of various metal ions at (A) 392 and (B) 484 nm. Data are acquired from Figure 1 and normalized to those prior to the addition of metal ions.


dx.doi.org/10.1021/la202424q |*Langmuir* 2011, 27, 12636–12641

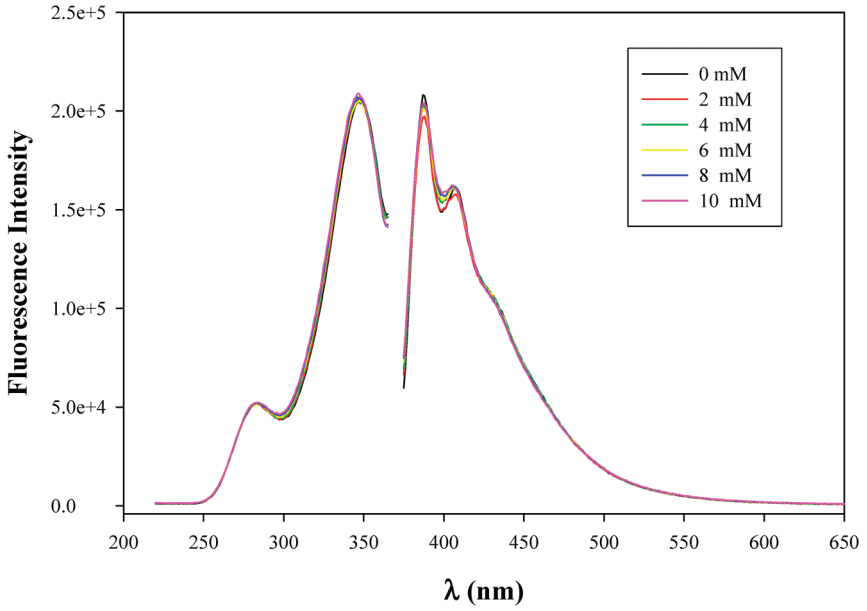


**Figure 3.** Fluorescence spectra of Ru═APyCE nanoparticles (2 mL, 0.05 mg/mL in DMF) with the addition of varied amounts of $KClO_4$ in DMF (0.1 M). The final concentrations of $K^+$ are listed in the legend. The excitation wavelength is set at 349 nm.

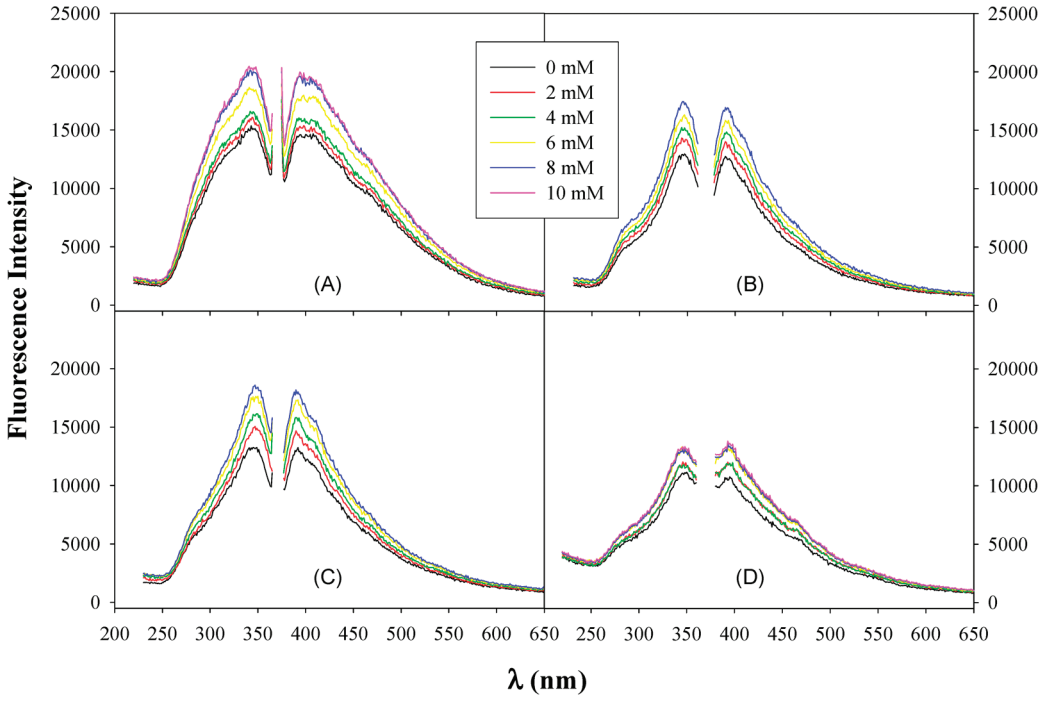


**Figure 4.** Fluorescence spectra of Ru═CE nanoparticles (2 mL, 0.05 mg/mL in DMF) with the addition of various amounts of metal salts in DMF (0.1 M): (A) $LiClO_4$, (B) $NaClO_4$, (C) $KClO_4$, and (D) $Mg(ClO_4)_2$. The final concentrations of the metal ions are listed in the legend. The excitation wavelength is set at 345 nm.

an order of magnitude weaker than that of Ru═VPyCE nanoparticles (Figure 1). This indicates that the Ru═VPyCE fluorescence is primarily from the pyrene moieties and the enhancement of the particle fluorescence is largely due to the chemical gating effect through the binding of metal ions by the crown ether cavity.

With respect to the possible cross interactions between the particle-bound pyrene and (benzo)crown ether moieties, we first investigated the fluorescence properties of the pyrene-crown ether conjugate (**2**). As shown in the Supporting Information (Figure S2), **2** exhibited apparent fluorescence characteristics, with a prominent excitation peak at 384 nm and an emission peak at 463 nm, and upon the introduction of metal ions into the compound solution, the fluorescence intensity increased markedly. As mentioned earlier, this may be accounted for by the encapsulation of metal ions in the crown ether cavity, where the positively

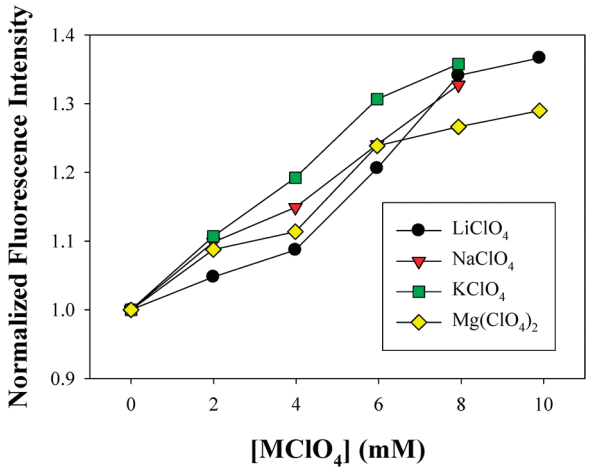


**Figure 5.** Variation of the emission intensity of the Ru═CE nanoparticles with the addition of various metal ions. Data are acquired from Figure 4 and normalized to those prior to the addition of metal ions.

charged ions raised the oxidation potential of the dialkoxy benzene of the crown and thus impeded photoinduced electron transfer to the excited pyrene moieties, as reported previously.[19,21−25] Therefore, we also excited the Ru═VPyCE nanoparticles at 384 nm and measured the fluorescence emission, where the profiles were largely featureless and the intensity was more than 1 order magnitude lower than that observed from the pyrene moieties (Figure S3). Again, this indicates that the contribution to the observed fluorescence profiles (Figure 1) from the conjugation between the pyrene and (benzo)-crown ether moieties on the nanoparticle surface is minimal. In essence, the lack of apparent conjugation between the pyrene and (benzo)crown ether moieties on the nanoparticle surface implies that intraparticle extended conjugation is likely to occur only for functional moieties with similar electronic energy structures, which may serve as a fundamental guideline for further and more complicated manipulation of the nanoparticle electronic and optical properties.

## CONCLUSIONS

In this study, by the cofunctionalization of carbene-stabilized ruthenium nanoparticles with pyrene and (benzo)crown ether moieties through Ru═carbene $\pi$ bonds, we demonstrated that selective ion binding of the crown ether cavity might be exploited as an effective chemical gating mechanism to regulate the energy of the nanoparticle core electrons and hence the intraparticle extended conjugation between the particle-bound pyrene moieties, as manifested in fluorescence measurements. The results showed that the chemical manipulation was achieved by the through-bond pathway whereas the through-space (electrostatic) contribution was minimal. Importantly, the electronic energy structure of the functional moieties is a critical factor in determining the effectiveness of conjugation between the particle-bound groups.

## ASSOCIATED CONTENT

**Supporting Information.** Experimental details of the synthesis of the pyrene−crown ether conjugate (**2**), NMR spectra of the Ru═VPyCE, Ru═APyCE, and Ru═CE nanoparticles after the nanoparticle cores were dissolved by dilute KCN and the organic components were collected for NMR measurements, and fluorescence spectra of **2** and Ru═VPyCE nanoparticles at different excitation wavelengths. This material is available free of charge via the Internet at http://pubs.acs.org.

## AUTHOR INFORMATION

### Corresponding Author

*E-mail: shaowei@ucsc.edu.

### Present Addresses

[†]State Key Laboratory of Electroanalytical Chemistry, Changchun Institute of Applied Chemistry, Chinese Academy of Sciences, Changchun, Jilin 130022, PR China.

## ACKNOWLEDGMENT

This work was supported in part by the National Science Foundation through grants CHE-1012256 and CHE-0832605 and by the ACS Petroleum Research Fund (49137-ND10).

## REFERENCES

(1) Schmid, G. *Chem. Rev.* **1992**, *92*, 1709–1727.
(2) Murray, R. W. *Chem. Rev.* **2008**, *108*, 2688–2720.
(3) Daniel, M. C.; Astruc, D. *Chem. Rev.* **2004**, *104*, 293–346.
(4) Chen, W.; Chen, S. W.; Ding, F. Z.; Wang, H. B.; Brown, L. E.; Konopelski, J. P. *J. Am. Chem. Soc.* **2008**, *130*, 12156–12162.
(5) Chen, W.; Zuckerman, N. B.; Kang, X. W.; Ghosh, D.; Konopelski, J. P.; Chen, S. W. *J. Phys. Chem. C* **2010**, *114*, 18146–18152.
(6) Chen, W.; Zuckerman, N. B.; Lewis, J. W.; Konopelski, J. P.; Chen, S. W. *J. Phys. Chem. C* **2009**, *113*, 16988–16995.
(7) Chen, W.; Zuckerman, N. B.; Konopelski, J. P.; Chen, S. W. *Anal. Chem.* **2010**, *82*, 461–465.
(8) Chen, W.; Pradhan, S.; Chen, S. W. *Nanoscale* **2011**, *3*, 2294–2300.
(9) Pruchnik, F. P. *Organometallic Chemistry of the Transition Elements*; Plenum Press: New York, 1990.
(10) Tsutsui, M.; Courtney, A. *Adv. Organomet. Chem.* **1977**, *16*, 241–282.
(11) Ding, F. Z.; Wang, H. B.; Wu, Q.; Van Voorhis, T.; Chen, S. W.; Konopelski, J. P. *J. Phys. Chem. A* **2010**, *114*, 6039–6046.
(12) Ding, F. Z.; Chen, S. W.; Wang, H. B. *Materials* **2010**, *3*, 2668–2683.
(13) Kang, X. W.; Chen, S. W. *Angew. Chem., Int. Ed.* **2010**, *49*, 9496–9699.
(14) Chou, F. F.; Shih, J. S. *J. Chin. Chem. Soc.* **2002**, *49*, 599–605.
(15) Chen, W.; Davies, J. R.; Ghosh, D.; Tong, M. C.; Konopelski, J. P.; Chen, S. W. *Chem. Mater.* **2006**, *18*, 5253–5259.
(16) Lamb, J. D.; Izatt, R. M.; Swain, C. S.; Christensen, J. J. *J. Am. Chem. Soc.* **1980**, *102*, 475–479.
(17) Pedersen, C. J.; Frensdor, H. K. *Angew. Chem., Int. Ed.* **1972**, *11*, 16–25.
(18) Izatt, R. M.; Rytting, J. H.; Nelson, D. P.; Haymore, B. L.; Christen, J. J. *Science* **1969**, *164*, 443–444.
(19) Gromov, S. P.; Ushakov, E. N.; Vedernikov, A. I.; Lobova, N. A.; Alfimov, M. V.; Strelenko, Y. A.; Whitesell, J. K.; Fox, M. A. *Org. Lett.* **1999**, *1*, 1697–1699.
(20) Chaudhuri, M. K.; Ganguly, S. C. *J. Phys. C: Solid State Phys.* **1969**, *2*, 1560–1565.
(21) Valeur, B.; Leray, I. *Coord. Chem. Rev.* **2000**, *205*, 3–40.
(22) Gromov, S. P.; Vedernikov, A. I.; Ushakov, E. N.; Alfimov, M. V. *Russ. Chem. Bull.* **2008**, *57*, 793–801.
(23) Gromov, S. P.; Vedernikov, A. I.; Ushakov, E. N.; Lobova, N. A.; Botsmanova, A. A.; Kuz'mina, L. G.; Churakov, A. V.; Strelenko, Y. A.; Alfimov, M. V.; Howard, J. A. K.; Johnels, D.; Edlund, U. G. *New J. Chem.* **2005**, *29*, 881–894.
(24) Shin, E. J. *Chem. Lett.* **2002**, 686–687.
(25) Shizuka, H.; Takada, K.; Morita, T. *J. Phys. Chem.* **1980**, *84*, 994–999.